Bio-based ether solvent and ionic liquid electrolyte for sustainable sodium–air batteries

Pierre L. Stigliano,[1,2] Nagore Ortiz-Vitoriano,*[3,4] Lidia Medinilla,[3] Jason E. Bara,[5] Juan Miguel López del Amo[3], Luis Lezama[6], Maria Forsyth[1], David Mecerreyes,[2,4] Cristina Pozo-Gonzalo*[1]

[1]Institute for Frontier Materials, Deakin University, Geelong, Victoria 3216, Australia

[2]POLYMAT, University of the Basque Country UPV/EHU, 20018, Donostia-San Sebastian, Spain

[3]Centre for Cooperative Research on Alternative Energies (CIC energiGUNE), Basque Research and Technology Alliance (BRTA), Alava Technology Park, Albert Einstein 48, Vitoria-Gasteiz 01510, Spain

[4]Ikerbasque, Basque Foundation for Science, María Díaz de Haro 3, 48013 Bilbao, Spain.

[5]The University of Alabama, SERC 3072E Box 870203, Tuscaloosa, AL 35487, USA

[6]Departamento de Química Orgánica e Inorgánica, Facultad de Ciencia y Tecnología, Universidad del País Vasco, UPV/EHU, Bº Sarriena s/n, 48940 Leioa, Spain

*Corresponding author: Nagore Ortiz-Vitoriano (email: nortiz@cicenergigune.com), Cristina Pozo-Gonzalo (email: cpg@deakin.edu.au).

ABSTRACT

Sodium-air batteries (SABs) are receiving much attention in the last years due to their high theoretical high energy density (up to 1105 Wh kg^{-1}). However, most of the studies on this technology are still based on organic solvents, in particular diglyme, a chemical considered highly flammable and toxic for the unborn child. Thus, the potential of the greener and low-toxic solvent 1,2,3 trimethoxypropane (TMP) as an alternative electrolyte to diglyme for SABs has been investigated for the first time in this publication. Through this work, it was found the reactivity of tertiary carbon present in TMP towards bare sodium metal. The addition of N-butyl-N-methylpyrrolidinium bis(trifluoromethylsulfonyl)imide ([C_4mpyr][TFSI]) as co-solvent proved to be effective to limit the reactivity. Moreover, a Na-β-alumina disk was employed as anode protection, to separate TMP-based electrolyte and sodium metal. The new cell design resulted in improved cell performance: discharge capacities of up to 1.92 and 2.31 mAh cm^{-2}, for 16.6 mol% NaTFSI in TMP and 16.6 mol% NaTFSI in TMP/[C_4mpyr][TFSI], respectively. By means of SEM, Raman and ^{23}NMR techniques NaO_2 cubes as the major discharge product for both electrolyte compositions were identified. Moreover, it was observed that the hybrid electrolyte hindered the formation of side-products during discharge (ratio NaO_2 to side-products in the hybrid electrolyte is 2.4 in comparison with the TMP based electrolyte 0.8) and a different charge mechanism for the dissolution of NaO_2 cubes for each electrolyte was observed. The findings of this work show the high potential of TMP as a base solvent for SABs, and the importance of careful electrolyte composition design, in order to step towards greener and less toxic batteries.

INTRODUCTION

Sodium-air batteries (SABs), also known as sodium-oxygen batteries, are a relatively new technology that it is attracting a great deal of attention due to their high theoretical energy density, 1605 Wh kg^{-1} or 1105 Wh kg^{-1} based on sodium peroxide (Na_2O_2) or sodium superoxide (NaO_2) discharge products, respectively.[1] SABs are, therefore, suitable for a wide range of applications such as electric vehicles,

renewable energy systems, and grid-level energy storage. In comparison, lithium-ion batteries (LIBs), the most diffused current battery technology, provides a practical energy density of ~ 250 Wh kg^{-1},[2] thus SABs could achieve an energy density 4-5 times higher than of LIBs. Another advantage of SABs is the low cost related to the active materials, sodium and oxygen, and this technology not requiring scarce elements like cobalt. Sodium is the 4th most abundant element on earth and can be extracted environmentally ethically and at a fraction of the cost of lithium metal. Additionally, aluminium current collector can be used, due to the non-reactivity with sodium, enabling lighter batteries. All these factors contribute to the lower cost of SABs compared to LIBs (200 \$ kW^{-1} h^{-1} versus 350–500 \$ kW^{-1} h^{-1} for LIBs).[3,4]

SABs are generally composed by three components, sodium metal as anode, an air cathode and a separator impregnated with an electrolyte. In a very simplified manner, during the discharge process, the sodium metal anode is oxidized releasing Na^+ that travels through the electrolyte towards the cathode. At the same time, O_2 is reduced (oxygen reduction reaction, ORR) at the three-phase boundary where liquid (electrolyte), gas (oxygen) and solid (air cathode) meet and in the presence of Na^+ in the electrolyte and ideally forms NaO_2 and/or Na_2O_2. During the charge process, the opposite processes take place, Na plating on the anode and oxygen evolution oxygen evolution reaction (OER) in the cathode. Although SABs theoretical energy density when Na_2O_2 (1605 Wh kg^{-1}) is formed is higher compared to NaO_2 (1105 Wh kg^{-1}), the latter is preferred as leads to lower overpotential and better cyclability of the battery.[5,6]

The main technological challenges of SABs are ascribed to low rechargeability, dendrite growth, and reactive nature of electrogenerated species, especially superoxide anion, that reacts with the main components of the battery [5,7–9] The chemical composition of the electrolyte in SABs has proven to be fundamental to control the chemical composition and morphology of the discharge products. This is of great importance as the discharge product influences the energy density, overpotential and cyclability of SABs, [10–15] therefore research on new electrolyte systems has become a hot topic in the last years.[10–15] The first family of electrolytes studied, was mostly organic carbonate-based electrolytes; however, the discharge products were usually a combination of Na_2O_2 and side products mostly composed of Na_2CO_3.[1] The side-products in this electrolyte are originated as a result of nucleophilic attack by $O_2^{\bullet-}$ to the ethereal carbon of CH_2 groups in carbonate-based solvents.[16]

After that Hartmann et al.[17] demonstrated the formation of sodium superoxide as the main discharge product when using ether-based electrolytes which resulted in low charge overpotential. Thus, the trend in research shifted from carbonate to ether-based organic solvents. Lutz et al.[18] reported the ORR process by modifying the glyme chain length, emphasizing the need of a low desolvation barrier for effective NaO_2 development. Ortiz-Vitoriano et al.[19] demonstrated how size and dynamics of glymes impact both ORR (discharge) and OER (charge) in SABs. Moreover, they showed the best outcomes in terms of transport and reaction kinetics were achieved by diglyme (DGME), thanks to its optimal balance in stability, viscosity, and coordination structure. Now, DGME is being widely employed, resulting in high discharge capacity and cyclability of the cell. [19–21] However, the main issues related to the use of diglyme are its volatility, flammability, and, more importantly, toxicity. In particular, DGME is connected with potential hazard for fertility and unborn child, posing a high risk when used in batteries, especially in the case of SABs which are open to air for their design.

In order to improve the safety and stability of SABs, ionic liquids (IL) have been investigated in this field. [22,2319–21] ILs are composed of an organic cation and either an organic or inorganic anion. This family of solvents stands out for their low volatility, non-flammability, high ionic conductivity and electrochemical stability.[11,22–25] Although ionic liquids proved to stabilize the superoxide anion, thus achieving preferential formation of NaO_2 as discharge product, the main issue of IL-based electrolytes

in SABs batteries is the limited discharge capacity especially at room temperature probably related to the viscosity of these systems.[11,12,26]

Hybrid electrolytes, which combine the advantages of organic solvents and ionic liquids, have been explored as potential electrolytes for SABs. This new class of electrolyte can combine the discharge capacity of organic solvents and the higher physicochemical and electrochemical stability of ILs.[27–29] In SABs, the use hybrid electrolytes based on diglyme and a pyrrolidinium-based ILs has been demonstrated which resulted in high stability towards the superoxide anion, oxygen and moisture, and more importantly the discharge products were more homogeneous in size (≈ 3.5 µm) and covering (3.1 cubes mm^{-2}).[13,28–30] However, the development of alternative hybrid electrolytes is necessary to address the toxicity which characterizes DGME, while maintaining similar physicochemical properties. Global current research has focused on greener based electrolytes and good example is 1,2,3-trimethoxypropane (TMP), which is a low toxic, bio-sourced constitutional isomer of diglyme, synthesized through the etherification of glycerol.[31]

Since TMP was originally synthesized, several uses for this solvent have been explored, including oxygenated bio-sourced additive for fuels, solvent for the reduction of organic functions, and CO_2 capture. Bara et al.[32] further investigated the thermophysical properties of TMP and simulated the ability of TMP to dissolve and coordinate metal cations such as Li^+, an important feature for electrolyte solvents as the solvation determines chemical and electrochemical environment of ions and the transport properties, which ultimately affect battery performance. They found the presence of Li^+ induces a crown-like coordination with the oxygen in the TMP molecule, similar to DGME. The ability to dissolve and conduct Li^+ through TMP was verified by Alvarez-Tirado et al.[33] by applying this new solvent to lithium-air batteries as liquid electrolyte or as plasticizer for gel polymer electrolytes. The results obtained showed promising discharge capacity (2.5 mAh cm^{-2} in liquid electrolyte) and charge overpotential <±0.04 V.

In this work, we report, for the first time, the application of TMP as an organic solvent to substitute diglyme in SABs. Furthermore, TMP was mixed with the ionic liquid N-butyl-N-methylpyrrolidinium bis(trifluoromethylsulfonyl)imide ([C_4mpyr][TFSI]), to investigate the potential of TMP-based hybrid electrolyte. We have found that although TMP reacted toward sodium metal, the hybrid electrolyte partially hindered the reactivity towards sodium metal. Strategies were explored in this work to protect the sodium metal by using an inorganic material, Na-β-Alumina disk. Through the cell design with anode protection, high discharge capacities up to 2.3 mAh cm^{-2} were achieved and the main discharge product obtained was NaO_2 in cubic shape which deposited on the air cathode. These results pave the way for the application of TMP as a substitute of diglyme in sodium-air batteries, and sodium-based batteries in general, avoiding the high risk related to diglyme and resulting in greener and safer batteries.

EXPERIMENTAL SECTION

Materials

Glycerol (>99.7%) and KOH (pellets, ACS grade) were purchased from BDH. DMS Dimethyl sulfate (DMS, (>99%) was purchased from Sigma- Aldrich. Tetrabutylammonium hydrogensulfate (TBAHS, TBAHS (98%) was purchased from Baker. All chemicals were used as received.

Sodium bis(trifluoromethylsulfonyl)imide (NaTFSI, Solvionic, 99.9%), N-butyl-N-methylpyrrolidinium bis(trifluoromethylsulfonyl)imide ([C_4mpyr][TFSI], Solvionic, 99.9%) were dried in Buchi oven overnight at 180 °C and 50 °C, respectively; and stored inside an Ar glovebox (ppm O_2 < 0.1, ppm H_2O < 0.1, Jacomex, France).

The TMP and TMP/[C_4mpyr][TFSI] IL electrolytes with 16.6 mol% NaTFSI salt (1.4M and 1.15 M, respectively) were prepared in Ar glovebox and the amount of electrolyte used in each experiment was 200 µL.
The water content of the electrolytes was measured inside the glove box via Karl–Fischer titration (Metrohm KF 831 Karl Fischer Coulometer) and was less than 20 ppm.

Synthesis of 1,2,3-Trimethoxypropane

1,2,3-Trimethoxypropane (TMP) was synthesized from glycerol, KOH and DMS according to the procedure described by Sutter et al. [31] After the reaction, pentane was added to the crude and the salts washed several times with pentane. The filtrate solution was evaporated in rotavapor. Water was extracted with $NaSO_4$ and CaH_2 and subsequently 1,2,3-trimethoxypropane was obtained from the filtrate through distillation at 100 mbar/64-66 °C. The final product was stored in Ar glovebox (ppm O_2 < 0.1, ppm H_2O < 0.3) and further dried with molecular sieves (4 Å) for two weeks before use. The water content was measured via Karl–Fischer titration (Metrohm KF 831 Karl Fischer Coulometer) and was less than 20 ppm.

Instrumentation and techniques

For ionic conductivity, an Autolab 302N potentiostat galvanostat (Metrohm AG) equipped with a temperature controller (Microcell HC station) was used to measure the electrolytes ionic conductivity. The liquid electrolytes were placed in a silicone O-ring between two stainless steel electrodes (surface area = 0.5 cm^2) and measurements were obtained at different temperatures (25 - 95 °C) in the range of 10^6-10^{-1} kHz, with 10 mV amplitude.

A 2-electrode Swagelok-type cell was employed for electrochemical testing. The cell parts were dried at 60 °C overnight and then transferred to an Ar-filled glovebox (H2O < 0.1 ppm, O2 <0.1 ppm; Jacomex, France) for assembling. The SAB cell was composed of a sodium metal disk (diameter = 12 mm, Sigma Aldrich). The sodium was cleaned using kimwipes inside the Ar glovebox. Carbon paper H23C6 cathode (diameter = 12 mm, Freundenberg), stainless steel mesh current collector (diameter = 12 mm, Alfa Aesar) and Celgard H2010 separators (diameter = 13 mm, Celgard (USA)), previously all dried under vacuum overnight at 70 °C, were used. For cell assembling, two Celgard separators soaked in 200 µL of electrolyte were placed on the sodium metal. The current collector was then placed on top of the carbon paper cathode. Finally, a spring was used to assure contact between the current collector and the Swagelok body which pressed into the oxygen inlet of the cell. .Once assembled, the cells were taken outside of the Ar glovebox and pressurized under pure oxygen (99.99% purity) for 10 s.

A Biologic-SAS VSP potentiostat was used for electrochemical experiments. The cells were left to rest for 8 hours at open circuit voltage and RT. Subsequently, a current density of ±75 µA cm^{-2} was applied. After electrochemical characterization, the cells were opened and the air cathodes cleaned in the glovebox with dry 1,2-dimethoxyethane before SEM, NMR and RAMAN characterization.

SEM measurements were performed by using a FEI Quanta 250 microscope operating at 5 kV. The electrodes were transferred from an Ar-filled glove box to the SEM using an air-tight holder to avoid air exposure.

Ex-situ solid state NMR experiments were conducted in a Bruker AVANCE III 500 MHz (11.7 T) wide bore spectrometer fitted with a 2.5 mm magic angle spinning (MAS) probe. The ^{23}Na spectra were

obtained using 1.5 µs hard pulses and a recycling delay of 4s. ^{23}Na chemical shifts were referenced to a 0.1 M NaCl solution at 0 ppm. All spectra were collected at a MAS rate of 20 KHz at room temperature. The carbon paper electrodes samples were cut into pieces after electrochemical characterization and placed into MAS rotors in an argon glove box.

Raman spectra were recorded using a Renishaw spectrometer (Nanonics Multiview 2000) focused with a 50x long working distance objective and operating at an excitation wavelength of 532 nm. The carbon paper electrodes after electrochemical characterization were sandwiched between two microscope glass slides and air-tight sealed using wax to avoid air exposure.

Electron paramagnetic resonance (EPR) measurements were performed at room temperature using a Bruker ELEXSYS E500 spectrometer operating at the X-band. The spectrometer was equipped with a super-high-Q resonator ER-4123-SHQ. Samples were placed into quartz glass capillary tubes with 0.6 mm inner diameter. Typical instrument settings were: center field, 3340. G; scan range, 100 G; time constant, 20.48 ms; modulation amplitude, 1.0 G; microwave power, 0.2 mW. The magnetic field was calibrated by a NMR probe and the frequency inside the cavity (~9.4 GHz) was determined with an integrated MW-frequency counter Data was collected and processed using the Bruker Xepr suite.

RESULTS AND DISCUSSION

In this work we investigate two electrolyte systems TMP and a hybrid electrolyte composed of NaTFSI salt and [C_4mpyr][TFSI]:TMP (1:4 molar ratio) solvent.

Figure **1**a shows the molecular structures of 1,2,3-Trimethoxypropane (TMP) which is an isomer of DGME (

Figure **1**b) with the main difference being that TMP has a branched structure and hence the presence of a tertiary carbon.

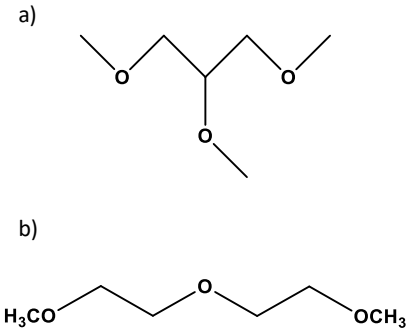

***Figure 1**. Molecular structure of a) 1,2,3-Trimethoxypropane (TMP) and b) diethylene glycol dimethyl ether (DGME).*

To investigate the influence of the electrolyte composition on the electrochemical performance of SABs, galvanostatic discharge experiments were carried out. Figure 2a shows the first deep discharge curves of the SABs using the two different electrolytes, 16.6 mol% NaTFSI in TMP and 16.6 mol% NaTFSI in TMP/[C_4mpyr][TFSI]. The cells were discharged at 75 µA cm^{-2} with a cut-off potential of 1.8 V at RT. The discharge profile presents an initial spike which is more pronounced in the case of the hybrid electrolyte TMP/[C_4mpyr][TFSI] (Figure 2 inset), probably related to mass transport limitations and to the nucleation of the discharge products generated on the air cathode.[30] The spike is followed by a plateau at 2.2 V for TMP-based electrolyte and a quick fading of the battery capacity. In the case of the hybrid electrolyte cell, the discharge capacity is larger than the TMP-based system with the potential decreasing progressively until reaching the cut-off potential. Nevertheless, both cells presented quite low discharge capacity in comparison with the state of the art normally in the range of 2.5 – 6 mAh cm^{-2} for diglyme and the hybrid electrolyte diglyme/[C_4mpyr][TFSI]. [12,13,30] It is interesting to note that the cell using TMP/[C_4mpyr][TFSI]-based electrolyte presented a discharge capacity of one order of magnitude larger (0.3 mAh cm^{-2}) than NaTFSI in TMP (0.025 mAh cm^{-2}). Note that those results present the opposed trend in discharge capacity with our previous studies when using DGME and hybrid electrolytes (DGME and several ionic liquids with also 16.6 mol% NaTFSI). The cells using the hybrid electrolyte always exhibited lower discharge capacity in comparison with those with the organic solvent DGME. [12,13,30]

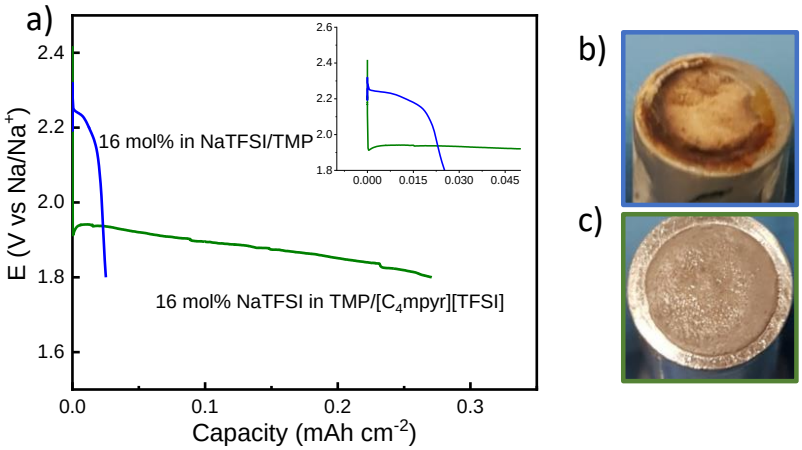

***Figure 2**. Discharge curves corresponding to 16.6 mol% NaTFSI in TMP (blue) and 16.6 mol% NaTFSI in TMP/[C_4mpyr][TFSI] (green) at RT. Applied current: 75 µA cm^{-2}, cut-off potential: 1.8 V; Sodium metal anodes after full discharge with b) 16.6 mol% NaTFSI in TMP and c) 16.6 mol% NaTFSI in TMP/[C_4mpyr][TFSI].*

A possible reason could be related to the passivation of the Na metal in contact with TMP. After disassembling the discharged cells, we observed the Na-metal electrode turned to red/orange coloration (Figure 2b) while remaining metallic when using the IL in the hybrid electrolyte mixture (Figure 2c). Lutz et al.[21] reported that the electrons generated during sodium oxidation (i.e. discharge process) can attack electrophilic centres such as those present on the carbon atoms of DGME. Therefore, the methylic group of DGME could be attacked by those electrons leading to the passivation of sodium metal and generating a SEI on the sodium metal composed of sodium-halides, organic ether-salts and carbonates.

In order to investigate the possibility of side reactions between sodium metal and TMP, a reactivity test with Na metal was performed by immerging a piece of metalling sodium in several solvent compositions; neat TMP, 16.6 mol% NaTFSI in TMP and 16.6 mol% NaTFSI in TMP/[C_4mpyr][TFSI]. The study was conducted under controlled conditions in an Ar glove box at room temperature. After 30 minutes, a reaction seems to occur between Na and most solvent compositions as a coloration is visible but in different degree (Figure 3a). In the case of TMP, a fast reaction occurs with Na and the red coloration is more intense compared to the other two samples. The mechanism proposed for the reaction between TMP and sodium, shown in Figure 3b, involves the nucleophilic attack on the tertiary carbon in TMP molecule by sodium, leading to the formation of a radical center on the carbon.

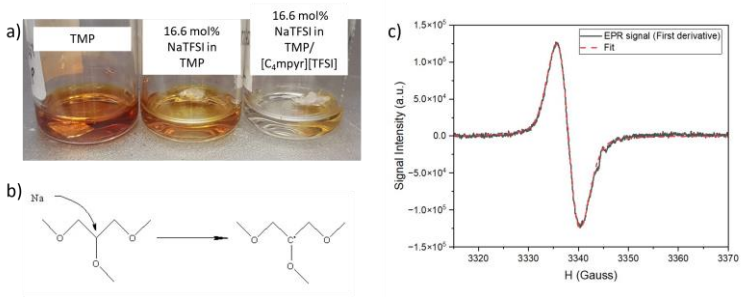

Figure 3. *a) Reactivity of sodium when immersed in TMP (left), 16.6 mol% NaTFSI in TMP (center), and 16.6 mol% NaTFSI in TMP/[C_4mpyr][TFSI] (right), after 30 minutes; b) Proposed mechanism for the reactivity of sodium with TMP, with the formation of a radical on the tertiary carbon in the TMP; c) molecule X-band room temperature EPR spectra of TMP after reaction with sodium for 30 minutes. The dotted line represents the best fit obtained using SpinFit.*

To corroborate the possible reaction mechanism, EPR analysis was performed to investigate the formation of radicals in the TMP molecule after the reaction with sodium metal. EPR spectroscopy is a powerful technique to investigate magnetic dipoles in a sample arising from the presence of unpaired electrons, such as in the case of radicals. When a specific value of magnetic field and electromagnetic radiation are applied on the sample, they interact (or resonate) with the unpaired electron(s). The spectrum in Figure 3c presents EPR signal vs magnetic field values (in Gauss), the first derivative of the resulting signal obtained was fitted to find the g-value. From the magnetic field value and electromagnetic wavelength, it is possible to obtain the g-value, which gives information related

to the paramagnetic centre's electronic structure. The g-value was obtained by the fitting of the first derivative of the EPR signal, using the Equation 1:

$$h\upsilon = g\mu_B B \quad \text{Eq:1}$$

where h is Plank's constant, μ is the frequency of the electromagnetic radiation (9.3645 GHz in our case), μ_B Bohr's magneton, and B the magnetic field value at which resonance occurs (3338 Gauss in our case).

In our study the formation of radicals was confirmed from the EPR experiment, with an g-factor of 2.0044. Usually, radicals centred on carbon atoms exhibit g values lower than our value (typically 2.0030)[34], however, higher values can be observed if functional groups with oxygen atoms are in the vicinity[35], as is the case of the TMP molecule. Due to the symmetry of the TMP, the proton on the tertiary carbon could be easily removed by nucleophilic attack similar to the proton on the beta-carbon in the imidazolium cation in the presence of superoxide anion.[25] To demonstrate that the radical formation observed by EPR is occurring on the tertiary carbon (Figure 3b), a TMP derivate was engineered by adding an ethyl pendant on the carbon, to obtain a quaternary carbon in the TMP molecule (Figure S1a). The new molecule, named trimethoxymethyl ethane, showed no reaction when sodium metal was immersed, even after 5 days (Figure S1b), confirming the radical-formation mechanism is located at the TMP tertiary carbon.

Considering the unwanted reactivity of TMP towards sodium, the SAB setup was redesigned to protect the sodium metal anode and hinder the reaction with TMP. Different strategies have been investigated in the literature to protect the sodium metal from oxygen electrogenerated species crossover during the discharge process, as well as remaining moisture from the oxygen gas or battery components (e.g. electrolyte, air cathode). In that regard, we have previously reported the use of an ionogel/ionic liquid bilayer electrolyte resulting in a high coulombic efficiency close to 100% with significant overpotential reduction.[36] Lin et al.[37] investigated the use of Alucone and NASICON-type solid-state electrolyte to protect Na-metal reducing superoxide crossover, suppressing dendrite growth, and improving efficient cyclability.

Herein we chose sodium-β-Alumina as Na-metal protective interlayer based on its high ionic conductivity, mechanical stability, and chemical stability against sodium; which makes this material interesting as solid electrolyte and sodium anode protector.[38–40] It was proved that Na-β-Alumina can achieve an ionic conductivity up to 5 mS cm^{-1} at room temperature[41] and a mechanical strength of 350 MPa.[19,42] Hence, a Na-β-Alumina disk was sandwiched between sodium metal and the separator soaked in the electrolyte, as showed in **¡Error! No se encuentra el origen de la referencia.**a.

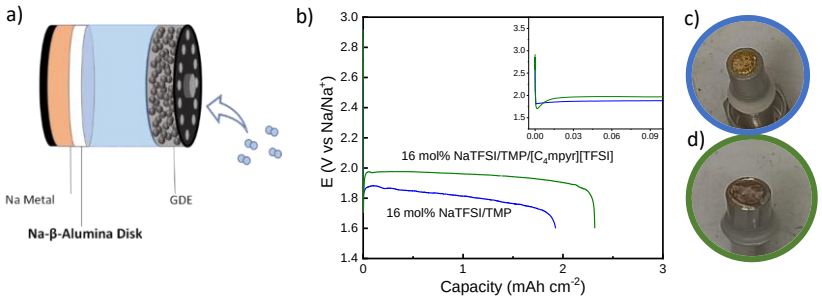

***Figure 4**: a) Representation of new cell design with Na-ß-Alumina as anode protector; b) Discharge curves corresponding to 16.6 mol% NaTFSI in TMP (blue) and 16.6 mol% NaTFSI in TMP/[C_4mpyr][TFSI] (green), with Na-ß-Alumina as anode protector. Discharge performed at RT. Applied current: 75 µAcm^{-2}, cut-off potential 1.6 V. The inset shows the initial spike during discharge; Sodium metal anodes with Na-ß-Alumina as anode protector after full discharge with (c) 16.6 mol% NaTFSI in TMP and (d) 16.6 mol% NaTFSI in TMP/[C_4mpyr][TFSI].*

Using the new design, the cells were discharged under the same experimental conditions as the initial cells (RT, 75 µA cm^{-2}). The discharge capacity was greatly improved, by at least one order of magnitude, achieving values of 1.92 and 2.31 mAh cm^{-2} for the cells with NaTFSI in TMP (**¡Error! No se encuentra el origen de la referencia.**b, blue) and NaTFSI in TMP/[C_4mpyr][TFSI] (**¡Error! No se encuentra el origen de la referencia.**b, green), respectively. The trend in discharge capacity is still in agreement with the experiments without the alumina disk where the hybrid electrolyte performed better in terms of discharge capacity. This still can be related to the presence of limited reactivity of Na with TMP. By close examination of the anode after the discharge process (**¡Error! No se encuentra el origen de la referencia.**c and d), we could observe the sodium metal anode presented a coloration for both electrolyte systems, meaning Na-β-Alumina could not achieve full protection of the anode, allowing the electrolyte to get in contact with sodium metal. The sodium metal presented a red coloration when in contact with the TMP as seen in the cells without anode protection. The cell employing the hybrid electrolyte presented certain coloration as well, which was no present in the absence of the Na-β-Alumina separator. This may be caused by the larger discharge time of the cell (8h rest + ≈30h discharge vs 8h rest + ≈30min discharge), which resulted in a longer contact between the hybrid electrolyte containing TMP and the sodium metal disk. As it will be explained later, the presence of side-reaction is the reason for resulting in lower discharge capacity values obtained in this work compared to DGME-based systems in literature for Na-O_2 and Li-O_2 batteries.[13,14,30,33]

The OCV for the cells with TMP-based electrolyte and with the hybrid electrolyte were 2.50 V and 2.70 V, respectively. After applying a discharge current of 75 µA cm^{-2}, the voltage quickly dropped to values below 2 V generating a spike (**¡Error! No se encuentra el origen de la referencia.**b inset) followed by a stable plateau. It has been reported that a more pronounced spike, like the one observed with NaTFSI in TMP/[C_4mpyr][TFSI], corresponds to greater nuclear distribution.[14,23] As shown below, this is in accordance with the discharge product size and distribution observed via SEM explained in detail in the following section (Figure 5). The voltage at which the cell with NaTFSI in TMP/[C_4mpyr][TFSI] discharges is slightly higher than that of NaTFSI in TMP, 1.97 V and 1.85 V at 0.5 mAh cm^{-2}, respectively. The discharge curve using NaTFSI in TMP is continuously lowering until complete discharge, while a more stable plateau is observed for the cell using NaTFSI in TMP/[C_4mpyr][TFSI].

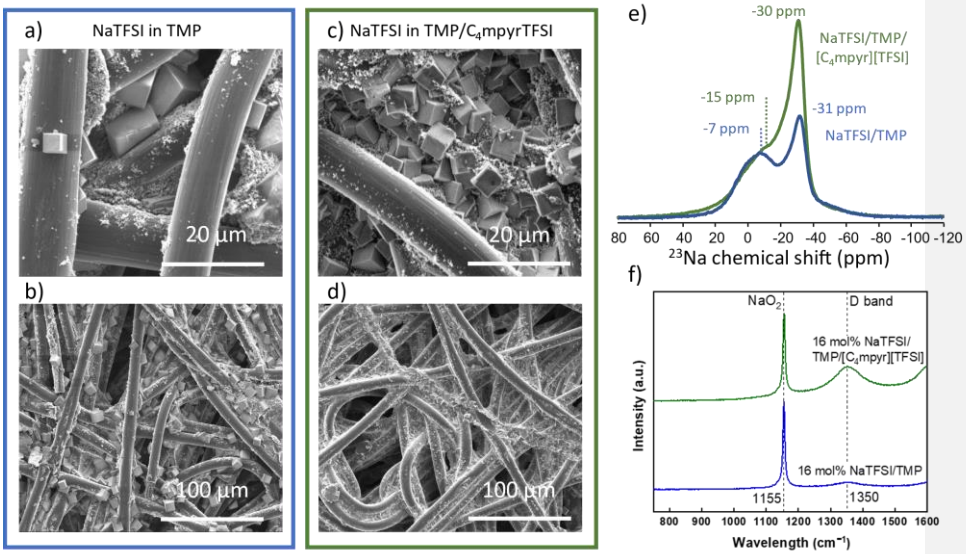

Figure 5*. SEM micrographs at different magnifications of the air cathodes after deep discharge corresponding to (a and b) 16.6 mol% NaTFSI in TMP and (c and d) 16 mol% NaTFSI in TMP/[C4mpyr][TFSI]; e) [23]Na Solid-state NMR spectra of air cathodes after deep discharge for 16.6 mol% NaTFSI in TMP (blue) and 16.6 mol% NaTFSI in TMP/[C4mpyr][TFSI] (green); f) RAMAN spectra of discharged air cathodes for 16.6 mol% NaTFSI in TMP (blue) and 16.6 mol% NaTFSI in TMP/[C4mpyr][TFSI] (green).*

The morphology, chemical composition, distribution, and crystallinity of the discharge products are important parameters in SABs as they control the electrochemical performance of the battery. After full discharge the air cathodes were characterized in detail by SEM, ^{23}Na solid state (ss) NMR, and Raman spectroscopy. SEM micrographs show the formation of NaO_2, which can be easily identified by the characteristic cubic shape[43], independently of the electrolyte composition (Figure 5a - d). However, differences in size and distribution were observed based on the chemical composition of the electrolyte. The NaO_2 cubes resulted larger in size (average size ≈ 9.7 ± 0.5 µm) and lower distribution, (covering: 2.9 10^{-2} cubes μm^{-2}) when using NaTFSI in TMP. In the case of NaTFSI in TMP/[C4mpyr][TFSI], smaller size cubes and more abundant were observed (average size ≈ 4.5 ± 0.4 µm, covering: 5.6 10^{-2} cubes μm^{-2}). The difference in size and distribution of discharge products observed is in accordance with the discharge voltage profile (**¡Error! No se encuentra el origen de la referencia.**b), where a deeper initial spike in the voltage is observed during discharge for the hybrid electrolyte.

As discussed above, NaO_2 is the main discharge product for both electrolytes, which was furtherly corroborated by NMR and Raman spectroscopy. ^{23}Na NMR spectra of the discharge air cathodes are shown in Figure 5e. In both spectra, a main signal is observed at -31 ppm for NaTFSI in TMP sample (blue line) and -30 ppm for NaTFSI in TMP/[C4mpyr][TFSI] sample (green line) and short longitudinal relaxation times of around 20ms. These values are in agreement with NaO_2 and its paramagnetic nature (Figure 5e) and in accordance with previously reported spectra of NaO_2.[44] The Raman spectra for both electrolytes in Figure 5f show the appearance of a peak at 1155 cm^{-1}, which is ascribed to

Comentado [CPG1]: In the ACS Energy Letters we have a value of -25 ppm and in the ACS applied mat and interf is -20 ppm

Comentado [CPG2R1]: We will need to acknowledge those changes in chemical shift

Comentado [NOV3R1]: Juan Miguel?

Comentado [CPG4]: Nagore, how do we see this in the NMR and what are the consequences?

Comentado [NOV5R4]: That is characteristic from NaO2 I guess, when JM revises he can have a look

NaO_2, according to literature. [45] Also, the absence of a peak in the 800 cm^{-1} region confirm the absence of the formation of sodium peroxide Na_2O_2 in the systems under study (full Raman spectra range in fig. S3).

Additional signals in the ^{23}Na ssNMR spectra observed in the region between 20 and -20 ppm are typically observed in ex-situ Na-air samples and related to the formation of side products during discharge.[46] Such signals are present on both electrolytes in Figure 5e. To estimate the relative intensities associated with the NaO_2 and side product resonances, the spectra were deconvoluted and are shown in Figure S2. Although a significant overlapping of signals precludes unambiguous assignments, there is a clearly higher concentration of NaO_2 relative to decomposition products in TMP/[C_4mpyr][TFSI] (2.4) respect to NaTFSI in TMP (0.8). The unambiguous identification of the secondary products by NMR is challenging due to the limited chemical shift range of ^{23}Na isotopes and their quadrupolar nature. The Raman spectrum of the cathode after full discharge in NaTFSI in TMP (full range is shown in Figure S3a) shows an additional peak at 745 cm^{-1}. This peak could be related to the presence of some residual NaTFSI on the surface of the cathode, in agreement with the work by Ponrouch et al when studying by RAMAN spectroscopy NaTFSI in various organic solvents.[48]

To further investigate the electrochemical properties and the reversibility of the systems, the cells were completely discharged and subsequently fully charged at 75 µA cm^{-2} and RT, with cut-off potentials of 1.6 V and 3.2 V for discharge and charge, respectively (Figure 6). NaTFSI in TMP achieved a full charge capacity of 1.51 mAh cm^{-2} with a Coulombic Efficiency (CE) of 79%, whereas NaTFSI in TMP/[C_4mpyr][TFSI] achieved 1.71 mAh cm^{-2} with a CE of 74%. Considering the size and purity of the discharge products it is difficult to discuss the lower CE for the hybrid system based in TMP, in comparison with the TMP.

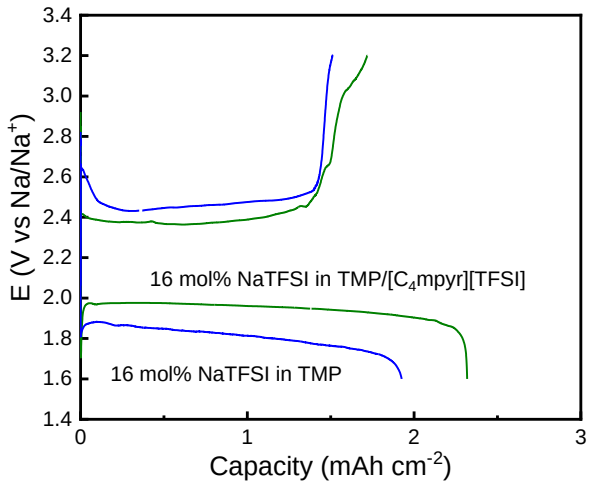

***Figure 6**. Galvanostatic full discharge charge profiles corresponding to 16.6 mol% NaTFSI in TMP (blue) and 16.6 mol% NaTFSI in TMP/[C_4mpyr][TFSI] (red), with Na-β-Alumina as anode protector. Discharge*

performed at RT. Applied current: 75 µAcm^{-2}, cut-off potential 1.6 V for discharge and 3.2 V for charge. The inset shows the initial spike during discharge and charge.

When comparing with our previous results, the charge capacity of the hybrid electrolytes based on DGME ranged from ~ 3 to 4 mAh cm^{-2} with CE higher than 80 %, therefore the electrochemical values related to the charge process in this study are somehow lower. This could be explained to some degree to the large presence of side products (55% for NaTFSI in TMP and 39% for NaTFSI in TMP/[C_4mpyr][TFSI]) in the TMP based systems.[13,14,19,30]

Moreover, other SABs based on protecting the sodium metal achieved higher CE than what obtained in other works. Lin et al.[37] achieved a coulombic efficiency of 95% when cycling a hybrid liquid/solid-state SAB based on Na@Alucone and NASICON. They also hypothesized the formation of an interfacial layer between the inorganic protective layer and the organic electrolyte, resulting from the reaction of the solid-state electrolyte and the NaO_2 discharge products. [37] In our case, the Na-β-Alumina disk might present limited internal resistance in comparison with liquid electrolytes, detrimental to coulombic efficiency. The influence on the cell overpotential due to the presence of Na-β-Alumina has been previously reported. Jiang et al.[49] reported an overpotential of 450 mV when Na-β-Alumina was used as solid electrolyte in SABs, as a consequence of the high internal resistance of the cell. High overvoltage is observed in both systems, NaTFSI in TMP and NaTFSI in TMP/[C_4mpyr][TFSI]. The cell using NaTFSI in TMP/[C_4mpyr][TFSI] cycled with the lowest overpotential (420 mV), calculated at 1 mAh cm^{-2}, while NaTFSI in TMP exhibited a larger overpotential of 650 mV. The higher overpotential observed in NaTFSI in TMP could be dictated by the formation of larger NaO_2 cubes and larger amount of irreversible products during discharge, as previously discussed. Moreover, given that the mechanical separator (alumina) still allows cross-over/contact between organic electrolytes and sodium metal (as it could be noticed by the coloration of the anode after discharge), the higher reactivity of NaTFSI in TMP (compared to NaTFSI in TMP/[C_4mpyr][TFSI]) could results in the formation of an unstable solid electrolyte interphase (SEI) forming on the sodium metal anode.[50,51]

It can be observed that the charge process trend in the two electrolytes differs, in NaTFSI in TMP we can find one plateau at 2.47 V, while NaTFSI in TMP/[C_4mpyr][TFSI] shows two plateau, the first one at 2.38 V and another starting at 3 V. The plateau for NaTFSI in TMP and first plateau for NaTFSI in TMP/[C_4mpyr][TFSI] are attributed to the dissolution (oxidation) of NaO_2. The appearance of a second plateau in the hybrid electrolyte has already been observed in literature[52] and is related to the oxidation of side-products forming during discharge, whose nature could not be fully disclosed, as mentioned above for the NMR spectra of discharged cathodes.

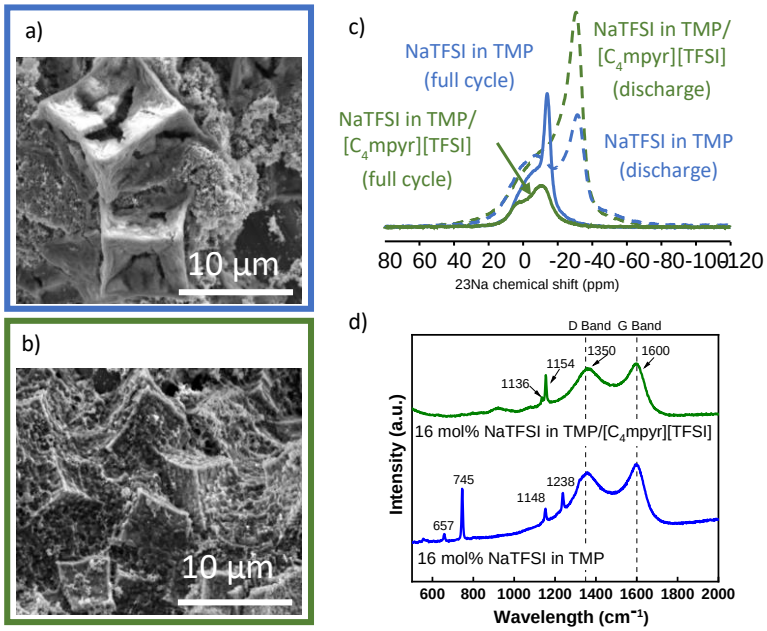

***Figure** 7. SEM micrographs of the charged air cathodes corresponding to (a) 16.6 mol% NaTFSI in TMP and (b) 16 mol% NaTFSI in TMP/[C4mpyr][TFSI]; c) ^{23}Na Solid-state NMR spectra of charged and cycled air cathodes for 16.6 mol% NaTFSI in TMP (blue) and 16 mol% NaTFSI in TMP/[C4mpyr][TFSI] (green). Solid lines refer to cathodes after discharge and dotted lines after full cycle; d) RAMAN spectra of charged air cathodes for 16.6 mol% NaTFSI in TMP (blue) and 16 mol% NaTFSI in TMP/[C4mpyr][TFSI] (green).*

After the full cycle, the air cathodes were characterized by means of SEM, ^{23}Na ssNMR, and RAMAN (Figure 7). The SEM micrographs show the presence of cubic structure on the air cathode but deconstructed in different ways depending on the electrolyte.

The cells using only TMP lead to the formation of hollow structures after charge, where only the outer shell of the cubes remained. The cubes, compared to the ones observed after discharge, appear to be marginally smaller (8.6 ± 0.7 µm vs 9.7 ± 0.5 µm). This behaviour during charge has been already reported, with core-shell structure dissolution during charge, and the removal of the core first.[53–55] It was found that initially during charge the core of the NaO_2 cubes dissolves and simultaneously there is the formation of carbonate phase on the outer shell. The formation of the carbonate outer shell was attributed to possible presence of oxygen singlets, species highly reactive and involved in many organic reactions.

In case of NaTFSI in TMP/[C4mpyr][TFSI] the cubes seems to be dissolved and a film covering the cubes has been formed. The cubes observed, differently from the case of NaTFSI in TMP, appear to the same size (4.8 ± 0.4 µm vs 4.5 ± 0.4 µm). It cannot be observed any signs of core-shell dissolution, as the

presence of cracks of the cubes faces is not revealed, although the presence of a film covering the products could hide the occurrence of such cracks. The formation of an additional film in the cathode could be related to the formation of a cathode electrolyte interphase due to the presence of the IL in the electrolyte.[56] To be the best of our knowledge, this type of deconstruction of the NaO_2 cubes has not been previously observed.

The ^{23}Na solid state NMR spectra, after the full cycle, shows the completely disappearance of the peak at -30 ppm which was assigned to NaO_2 (Figure 7c), and only the side product region between 20 and -20 ppm remained which has been split now into two peaks. The partial narrowing of the resonances assigned to secondary products in these spectra can be assigned to well defined local environments as expected by increased crystallinities of the compounds present.[46] This is in agreement with the observation of well-defined signals in the Raman spectra of these materials (Figure 7d).

The cells using the TMP electrolyte, presented a more complex combination of side products leading to 4 different peaks in the RAMAN spectrum (1152, 1237, 745 and 657 cm^{-1}). In the case of the hybrid electrolyte, two peaks corresponding to $Na_2O_2 \bullet H_2O$ at 1136 cm^{-1} and NaO_2 at 1154 cm^{-1} are observed. This is quite interesting as sodium peroxide was not observed during the discharge process. Most likely NaO_2 was reduced on the surface of the air cathode to the peroxide form. It is interesting that those products were not observed by ^{23}Na Solid-state NMR.

CONCLUSION

In this work, we have investigated for the first time the potential of TMP as a greener low-toxic substitute of diglyme as electrolyte for sodium-air batteries. Using neat TMP as electrolyte resulted in high reactivity towards bare sodium metal, producing undesired side reactions. The reaction mechanism was proved to be centred at the TMP tertiary carbon through the formation of a radical intermediary, as demonstrated by EPR and functionalisation of the tertiary carbon. Incorporating $[C_4mpyr][TFSI]$ ionic liquid as co-solvent to form a hybrid electrolyte results in a higher stability electrolyte, reducing side-reactions with Na-metal anode. Using Na-beta alumina protective interface can further reduce the reaction of TMP towards sodium-metal, resulting in an improved cell performance. Discharge capacities of up to 1.92 and 2.31 mAh cm^{-2}, for 16.6 mol% NaTFSI in TMP and 16.6 mol% NaTFSI in TMP/$[C_4mpyr][TFSI]$, respectively, could be attained. SEM, Raman and ^{23}NMR technique has been employed to understand the complexity of the cycled products. Upon discharge, characteristic NaO_2 cubes form in both electrolyte systems with size and distribution similar to diglyme-based electrolytes. Similarly to what has been observed in previous works, the use of the hybrid electrolyte resulted in a more homogeneous deposition of smaller NaO_2 cubes during discharge and the formation of lower amounts of side-products, compared to TMP only (relative concentration of NaO_2 to side-products of NaTFSI in TMP/$[C_4mpyr][TFSI]$ is 2.4 respect to NaTFSI in TMP is 0.8). During the charge process, different dissolution process of the NaO_2 were observed for each electrolyte system. While in the case of the TMP neat electrolyte a core-shell dissolution mechanism was observed, in the case of the hybrid electrolyte the dissolution of NaO_2 involved the formation of Na_2O_2 and an additional CEI. The findings of this work highlight the potential of TMP as a base solvent for SABs, and the importance of careful electrolyte composition design, opening the way for greener and less toxic batteries.

Acknowledgments

This project has received funding from the European Union's Horizon 2020 research and innovation programme under the Marie Skłodowska-Curie grant agreement No 860403. N. Ortiz-Vitoriano acknowledges the R&D&I project PID2020-117626RA-I00 funded by MCIN/AEI/10.13039/501100011033 and Ramon y Cajal grant (RYC-2020-030104-I) funded by MCIN/AEI/10.13039/501100011033 and by FSE invest in your future.

REFERENCES

1. Sun, Q., Yang, Y. & Fu, Z. W. Electrochemical properties of room temperature sodium-air batteries with non-aqueous electrolyte. *Electrochem commun* **16**, 22–25 (2012).
2. Masias, A., Marcicki, J. & Paxton, W. A. Opportunities and Challenges of Lithium Ion Batteries in Automotive Applications. *ACS Energy Lett* **6**, 621–630 (2021).
3. Ha, S., Kim, J. K., Choi, A., Kim, Y. & Lee, K. T. Sodium-metal halide and sodium-air batteries. *ChemPhysChem* vol. 15 1971–1982 Preprint at https://doi.org/10.1002/cphc.201402215 (2014).
4. Abraham, K. M. How Comparable Are Sodium-Ion Batteries to Lithium-Ion Counterparts? *ACS Energy Lett* **5**, 3544–3547 (2020).
5. Landa-Medrano, I. *et al.* Sodium-Oxygen Battery: Steps Toward Reality. *Journal of Physical Chemistry Letters* **7**, 1161–1166 (2016).
6. Yadegari, H. & Sun, X. Sodium–Oxygen Batteries: Recent Developments and Remaining Challenges. *Trends in Chemistry* vol. 2 241–253 Preprint at https://doi.org/10.1016/j.trechm.2019.12.003 (2020).
7. Yadegari, H. *et al.* Sodium-Oxygen Batteries: A Comparative Review from Chemical and Electrochemical Fundamentals to Future Perspective. *Advanced Materials* **28**, 7065–7093 (2016).
8. Medenbach, L. *et al.* Origins of Dendrite Formation in Sodium–Oxygen Batteries and Possible Countermeasures. *Energy Technology* **5**, 2265–2274 (2017).
9. Lin, X. *et al.* The application of carbon materials in nonaqueous Na-O 2 batteries. *Carbon Energy* **1**, 141–164 (2019).
10. Tatara, R. *et al.* Tuning NaO2 Cube Sizes by Controlling Na+ and Solvent Activity in Na-O2 Batteries. *Journal of Physical Chemistry C* **122**, 18316–18328 (2018).
11. Azaceta, E. *et al.* Electrochemical Reduction of Oxygen in Aprotic Ionic Liquids Containing Metal Cations: A Case Study on the Na–O2 system. *ChemSusChem* **10**, 1616–1623 (2017).
12. Zhang, Y. *et al.* Elucidating the Impact of Sodium Salt Concentration on the Cathode-Electrolyte Interface of Na-Air Batteries. *Journal of Physical Chemistry C* **122**, 15276–15286 (2018).

13. Garcia-Quintana, L. *et al.* Unravelling the Role of Speciation in Glyme:Ionic Liquid Hybrid Electrolytes for Na−O2 Batteries. *Batter Supercaps* **4**, 513–521 (2021).

14. Garcia-Quintana, L. *et al.* Unveiling the Impact of the Cations and Anions in Ionic Liquid/Glyme Hybrid Electrolytes for Na–O2 Batteries. *ACS Appl Mater Interfaces* **14**, 4022–4034 (2022).

15. Aldous, I. M. & Hardwick, L. J. Solvent-Mediated Control of the Electrochemical Discharge Products of Non-Aqueous Sodium–Oxygen Electrochemistry. *Angewandte Chemie International Edition* **55**, 8254–8257 (2016).

16. Kim, J., Lim, H. D., Gwon, H. & Kang, K. Sodium–oxygen batteries with alkyl-carbonate and ether based electrolytes. *Physical Chemistry Chemical Physics* **15**, 3623–3629 (2013).

17. Hartmann, P. *et al.* A rechargeable room-temperature sodium superoxide (NaO2) battery. *Nat Mater* **12**, 228–232 (2013).

18. Lutz, L. *et al.* High capacity Na-O2 batteries: Key parameters for solution-mediated discharge. *Journal of Physical Chemistry C* **120**, 20068–20076 (2016).

19. Ortiz Vitoriano, N. *et al.* Goldilocks and the three glymes: How Na+ solvation controls Na–O2 battery cycling. *Energy Storage Mater* **29**, 235–245 (2020).

20. Black, R. *et al.* The Nature and Impact of Side Reactions in Glyme-based Sodium–Oxygen Batteries. *ChemSusChem* **9**, 1795–1803 (2016).

21. Lutz, L. *et al.* Role of Electrolyte Anions in the Na-O2 Battery: Implications for NaO2 Solvation and the Stability of the Sodium Solid Electrolyte Interphase in Glyme Ethers. *Chemistry of Materials* **29**, 6066–6075 (2017).

22. Rakov, D. A. *et al.* Engineering high-energy-density sodium battery anodes for improved cycling with superconcentrated ionic-liquid electrolytes. *Nature Materials 2020 19:10* **19**, 1096–1101 (2020).

23. Sano, H., Sakaebe, H., Senoh, H. & Matsumoto, H. Effect of Current Density on Morphology of Lithium Electrodeposited in Ionic Liquid-Based Electrolytes. *J Electrochem Soc* **161**, A1236–A1240 (2014).

24. Yang, Q. *et al.* Ionic liquids and derived materials for lithium and sodium batteries. *Chem Soc Rev* **47**, 2020–2064 (2018).

25. Islam, M. M. *et al.* Stability of superoxide ion in imidazolium cation-based room-temperature ionic liquids. *Journal of Physical Chemistry A* **113**, 912–916 (2009).

26. Pozo-Gonzalo, C. *et al.* Controlling the Three-Phase Boundary in Na–Oxygen Batteries: The Synergy of Carbon Nanofibers and Ionic Liquid. *ChemSusChem* **12**, 4054–4063 (2019).

27. Meisner, Q. J. *et al.* Impact of Co-Solvent and LiTFSI Concentration on Ionic Liquid-Based Electrolytes for Li-S Battery. *J Electrochem Soc* **167**, 070528 (2020).

28. Monti, D., Ponrouch, A., Palacín, M. R. & Johansson, P. Towards safer sodium-ion batteries via organic solvent/ionic liquid based hybrid electrolytes. *J Power Sources* **324**, 712–721 (2016).

29. Manohar, C. V. *et al.* Stability enhancing ionic liquid hybrid electrolyte for NVP@C cathode based sodium batteries. *Sustain Energy Fuels* **2**, 566–576 (2018).

30. Ortiz-Vitoriano, N. *et al.* Highly Homogeneous Sodium Superoxide Growth in Na-O2 Batteries Enabled by a Hybrid Electrolyte. *ACS Energy Lett* **5**, 903–909 (2020).

31. Sutter, M., Dayoub, W., Métay, E., Raoul, Y. & Lemaire, M. 1,2,3-Trimethoxypropane and Glycerol Ethers as Bio-Sourced Solvents from Glycerol. Synthesis by Solvent-Free Phase-Transfer Catalysis and Utilization as an Alternative Solvent in Chemical Transformations. *ChemCatChem* **5**, 2893–2904 (2013).

32. Barbosa, G. D., Bara, J. E. & Turner, C. H. Molecular simulation of glycerol-derived triether podands for lithium ion solvation. *Physical Chemistry Chemical Physics* **24**, 9459–9466 (2022).

33. Marta Alvarez-Tirado *et al.* 1,2,3-Trimethoxypropane: a bio-sourced glyme as electrolyte for lithium–O 2 batteries. *Green Chemistry* **24**, 6016–6025 (2022).

34. Qin, Y. *et al.* Persistent free radicals in carbon-based materials on transformation of refractory organic contaminants (ROCs) in water: A critical review. *Water Res* **137**, 130–143 (2018).

35. Woodward, J. R. Radical Pairs in Solution. *Progress in Reaction Kinetics and Mechanism* **27**, 165–207 (2002).

36. Ha, T. A. *et al.* High Coulombic Efficiency Na-O2 Batteries Enabled by a Bilayer Ionogel/Ionic Liquid. *Journal of Physical Chemistry Letters* **10**, 7050–7055 (2019).

37. Lin, X. *et al.* Reviving Anode Protection Layer in Na-O2 Batteries: Failure Mechanism and Resolving Strategy. *Adv Energy Mater* **11**, 2003789 (2021).

38. Wenzel, S. *et al.* Interfacial Reactivity Benchmarking of the Sodium Ion Conductors Na3PS4 and Sodium β-Alumina for Protected Sodium Metal Anodes and Sodium All-Solid-State Batteries. *ACS Appl Mater Interfaces* **8**, 28216–28224 (2016).

39. Lu, X., Lemmon, J. P., Sprenkle, V. & Yang, Z. Sodium-beta alumina batteries: Status and challenges. *JOM 2010 62:9* **62**, 31–36 (2010).

40. Fertig, M. P. *et al.* From High- to Low-Temperature: The Revival of Sodium-Beta Alumina for Sodium Solid-State Batteries. *Batter Supercaps* **5**, e202100131 (2022).

41. Yi, E., Temeche, E. & Laine, R. M. Superionically conducting β′′-Al2O3 thin films processed using flame synthesized nanopowders. *J Mater Chem A Mater* **6**, 12411–12419 (2018).

42. Ligon, S. C. *et al.* Performance analysis of Na-β″-Al2O3/YSZ solid electrolytes produced by conventional sintering and by vapor conversion of α-Al2O3/YSZ. *Solid State Ion* **345**, 115169 (2020).

43. Bi, X. *et al.* A Critical Review on Superoxide-Based Sodium–Oxygen Batteries. *Small Methods* **3**, 1800247 (2019).

44. Krawietz, T. R., Murray, D. K. & Haw, J. F. Alkali metal oxides, peroxides, and superoxides: A multinuclear MAS NMR study. *Journal of Physical Chemistry A* **102**, 8779–8785 (1998).

45. Hartmann, P. *et al.* A comprehensive study on the cell chemistry of the sodium superoxide (NaO2) battery. *Physical Chemistry Chemical Physics* **15**, 11661–11672 (2013).

46. Liu, T., Kim, G., Casford, M. T. L. & Grey, C. P. Mechanistic Insights into the Challenges of Cycling a Nonaqueous Na-O2 Battery. *Journal of Physical Chemistry Letters* **7**, 4841–4846 (2016).

47. Rudolph, W. W. & Irmer, G. Raman Spectroscopic Studies on Aqueous Sodium Formate Solutions and DFT Calculations. *J Solution Chem* **51**, 935–961 (2022).

48. Ponrouch, A. *et al.* Towards high energy density sodium ion batteries through electrolyte optimization. *Energy Environ Sci* **6**, 2361–2369 (2013).

49. Fathi Tovini, M. *et al.* A rechargeable all-solid-state sodium peroxide (Na2O2) battery with low overpotential. *J Phys D Appl Phys* **54**, 174005 (2021).

50. Wu, S. *et al.* Tailoring Sodium Anodes for Stable Sodium–Oxygen Batteries. *Adv Funct Mater* **28**, 1706374 (2018).

51. Zheng, X. *et al.* Sodium metal anodes for room-temperature sodium-ion batteries: Applications, challenges and solutions. *Energy Storage Mater* **16**, 6–23 (2019).

52. Kim, J. *et al.* Dissolution and ionization of sodium superoxide in sodium–oxygen batteries. *Nature Communications 2016 7:1* **7**, 1–9 (2016).

53. Landa-Medrano, I. *et al.* Architecture of Na-O2 battery deposits revealed by transmission X-ray microscopy. *Nano Energy* **37**, 224–231 (2017).

54. Sun, Q. *et al.* Visualizing the Oxidation Mechanism and Morphological Evolution of the Cubic-Shaped Superoxide Discharge Product in Na–Air Batteries. *Adv Funct Mater* **29**, 1808332 (2019).

55. Aldous, I. M. & Hardwick, L. J. Growth and dissolution of NaO2 in an ether-based electrolyte as the discharge product in the Na–O2 cell. *Chemical Communications* **54**, 3444–3447 (2018).

56. Do, M. P. *et al.* Effect of Conducting Salts in Ionic Liquid Electrolytes for Enhanced Cyclability of Sodium-Ion Batteries. *ACS Appl Mater Interfaces* **11**, 23972–23981 (2019).